atmosphere

MDPI

Article

Evaluation and Projection of Gale Events in North China

Rong Yuan [1], Qiuyue Li [2,*], Lingfang Wu [1], Miao Huo [1] and Yi Huang [1]

[1] Meteorological Center of Air Traffic Regulation of Civil Aviation in North China, Beijing 100621, China; yuan_rong01@126.com (R.Y.); karen_wlf@hotmail.com (L.W.); huomiao0826@163.com (M.H.); 520pheonix@163.com (Y.H.)
[2] Beijing Municipal Climate Center, Beijing 100089, China
* Correspondence: liqiuyue@bj.cma.gov.cn

Abstract: As an important weather extreme, gales greatly impact the air quality, agriculture, aviation, and renewable energy in North China. However, the spatial–temporal changes in gale events remain unknown in North China. In this study, using the ERA5 reanalysis with high spatiotemporal resolution and multi-model simulations from the Coupled Model Intercomparison Project Phase Six (CMIP6), we investigate the temporal changes, including daily, seasonal and decadal variations in gale events in North China between 1980 and 2021, and we project the changes in gale events in the mid and late 21st century under two shared socio-economic pathways (SSPs). The gale events show large spatial heterogeneity in frequency, with a high frequency of >25 days/year in central Inner Mongolia province, northern Hebei province, and northwestern Beijing. Over the past four decades, the gale events in North China have shown a decadal reversal, with a decrease between 1980 and 2006 and an increase between 2007 and 2014. Furthermore, the gale events show strong temporal variations in North China. For seasonal variation, the gale events exhibit double peaks, with the largest peak in April and the smallest peak in October. For daily variation, the gale events show a single peak, with the maximum from 10:00 to 16:00 local time in North China. Multi-model simulations from CMIP6 reveal a continuous decreasing trend of gale events in North China by the end of the 21st century under both SSP1-2.6 and SSP2-4.5 scenarios relative to the historical period. Our results provide comprehensive support for planning aviation, renewable energy, and agriculture in the future.

Keywords: gale event; spatial–temporal changes; North China

check for updates

Citation: Yuan, R.; Li, Q.; Wu, L.; Huo, M.; Huang, Y. Evaluation and Projection of Gale Events in North China. *Atmosphere* **2023**, *14*, 1646. https://doi.org/10.3390/atmos14111646

Academic Editors: Zhaobin Sun, Jun Yang and Ling Han

Received: 14 September 2023
Revised: 17 October 2023
Accepted: 26 October 2023
Published: 2 November 2023

Copyright: © 2023 by the authors. Licensee MDPI, Basel, Switzerland. This article is an open access article distributed under the terms and conditions of the Creative Commons Attribution (CC BY) license (https://creativecommons.org/licenses/by/4.0/).

1. Introduction

Climate extremes refer to a weather (climate) condition that deviates significantly from its mean state [1]. The observed evidence shows that most climate extremes, including heatwaves, droughts, and floods, have become more frequent and severe in recent decades as a result of anthropogenic climate warming [2–5]. For example, over the past few decades, 58–73% of land regions have shown a significant increase in compound drought and heatwaves due to anthropogenic emissions [6]. Meanwhile, modeling studies reported that the global weather and climate extremes are projected to increase by approximately two-fold compared to historical periods by the end of this century under a high emission scenario [7,8]. The increase is projected to exceed four-fold, particularly in densely populated regions, such as the United States, north Africa, and Asia [9–11].

As an important extreme weather event, gales significantly impact energy, the ecological environment, and aviation [12–14]. In terms of energy, while strong winds contribute to generating more wind energy, they also increase the load and risk of damage to the wind power equipment [15]. For agriculture, strong winds may break or damage the stems, branches, and fruits or disrupt pollination processes, resulting in reduced crop yield or even death [16]. Strong crosswinds or rapidly changing wind directions can make takeoff and landing challenging for aviation [17]. Furthermore, gale events can cause damage to

buildings, infrastructure, and vehicles. Fallen trees, damaged roofs, and toppled power poles can pose risks of personal injury and property loss. For example, Inner Mongolia experienced consecutive strong winds in mid-March 2021, with the highest wind force reaching level 11 and the instantaneous maximum wind speed approaching an almost 50-year record. Such powerful winds devastated a solar power array of nearly a hundred megawatts and caused soil erosion in arid areas [18,19], leading to severe sandstorm weather conditions in North China [20,21].

North China has a predominantly temperate monsoon climate (Figure 1). The average annual temperature is around 8–13 °C. The annual precipitation is around 400–800 mm. It is hot and rainy in the summer, which promotes crop growth. Therefore, North China is the largest agricultural region in China, accounting for more than 60% of wheat and 30% of maize yields [22,23]. Meanwhile, North China is an important transportation and wind farm hub [24] but has suffered from severe air pollution in recent years, posing a serious threat to human health [25–27]. Therefore, gale events are an important weather extreme in North China, influencing agriculture, aviation, energy, and air quality.

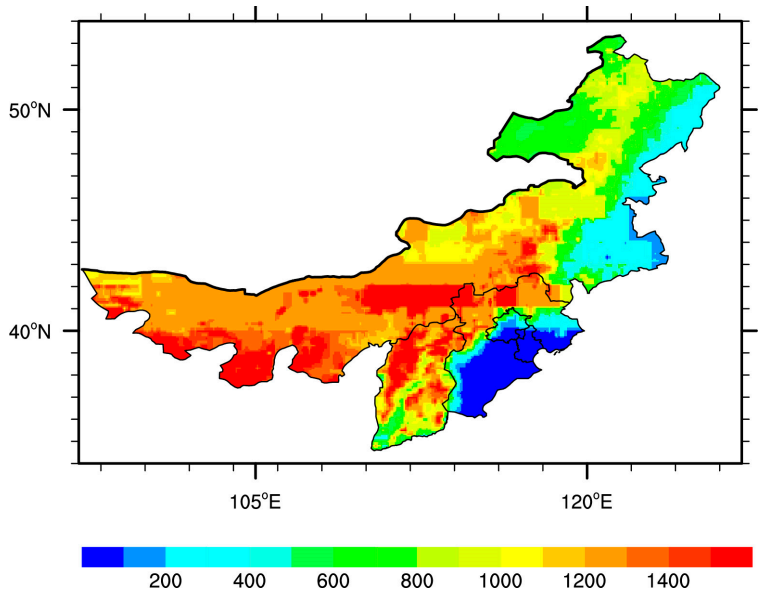

Figure 1. The study region of north China. The shadings represent the altitude.

Although Shi et al. [28] analyzed the decadal changes in gale weather events in the entirety of China and reported that the frequency of gale events showed a decreasing trend of 3.7 days/decade for China as a whole between 1959 and 2014, their study lacked the daily and seasonal variations and future projection of gale events, hindering the comprehensive assessment of gale weather events. In this study, using the hourly ERA5 reanalysis and combining daily model outputs from the Coupled Model Intercomparison Project Phase six (CMIP6), we evaluate the spatial–temporal changes in gale events over the historical period and project the changes in gale events under two future shared socio-economic pathways (SSP), including SSP1-2.6 and SSP2-4.5, by the mid-to-late 21st century in North China. Such a study will provide comprehensive support for planning agriculture, renewable energy, and flight distributions in North China.

2. Data and Methods

2.1. The ERA5 Reanalysis

In this study, we use the hourly ERA5 reanalysis with a high horizontal resolution of 0.25° × 0.25° to investigate gale events' spatial–temporal changes between 1980 and 2021 in North China. ERA5 is the fifth-generation reanalysis from the European Centre for Medium-Range Weather Forecasts (ECMWF; https://www.ecmwf.int/en/forecasts/

dataset/ecmwf-reanalysis-v5) (accessed on 1 January 2023), which replaced ERA-Interim as the next generation of representative satellite observational data on the global scale. ERA5 is generated by the Copernicus Climate Change Service (C3S) at the ECMWF. The ERA5 reanalysis has proven to be one of the best reanalysis datasets [29,30] and is widely used in risk assessments and climate change studies [31–33]. This study uses the instantaneous 10 m wind gust from the ERA5 variable to define the gale event in North China.

2.2. Model Outputs from CMIP6

The earth system model (ESM) is an important tool for projecting future climate change [34–36]. The predecessor of the Earth system model is the Climate System Model (CSM). The traditional climate system model mainly includes the atmospheric circulation, land surface physical, ocean, and sea ice systems. From the end of the last century to the beginning of this century, with the deepening of the research on global climate change, the Climate System Model has been continuously developed, and its field has been gradually expanded to the ecological and environmental systems of the Earth's surface, including land and marine ecosystems, atmospheric chemistry, aerosols, etc. At the present stage, the Earth system model is a mathematical model based on the physical, chemical, and biological processes in the various layers of the Earth, as well as the laws of material and energy exchange between them, which is then solved by numerical calculations and compiled into a large-scale comprehensive calculation program.

The Coupled Model International Comparison Program (CMIP) was initiated and organized by the World Climate Research Program (WCRP) Working Group on Coupled Modeling (WGCM) in 1995, with the initial aim of comparing the performance of the then limited number of global coupled climate models. CMIP6 has the largest number of participating models, the best-designed scientific experiments, and the largest amount of simulation data provided in more than 20 years of the CMIP program. In this study, we use model simulations from CMIP6 to project the changes in gale events in North China by the end of the 21st century. Due to ESM's lack of hourly output, we select the daily maximum near-surface wind speed (sfcWindmax) variable to define gale events in North China. Considering the availability of sfcWindmax, eight ESMs from CMIP6 are used in this study (Table 1). These ESMs provide simulations of the historical period and two future Shared Socio-economic Pathways (SSP), including SSP1-2.6 and SSP2-4.5. These SSPs represent alternative evolutions of future society in the absence of climate change or climate policy [37]. For example, SSP1-2.6 refers to a scenario combining SSP1-based socio-economic and RCP2.6-based energy-emissions-land use scenarios. SSP2-4.5 refers to a scenario combining SSP2-based socio-economic and RCP4.5-based energy-emissions-land use scenarios. In this study, the simulations in the historical period are used to evaluate the performance of ESMs in simulating gale events in North China, and the simulations in three future scenarios are used to project the changes of gale events in North China by the mid-to-late 21st century. To maintain consistent horizontal resolution, all model outputs are interpolated to a common resolution of $0.5^\circ \times 0.5^\circ$ using the bilinear interpolation method.

Table 1. Summary of eight CMIP6 models used in this study.

Model	Country	Resolution (Lat × Lon)
ACCESS-ESM1-5	Australia	145 × 192
AWI-CM-1-1-MR	Germany	192 × 384
BCC-CSM2-MR	China	160 × 320
CanESM5	Canada	64 × 128
FGOALS-g3	China	80 × 180
MIROC6	Japan	128 × 256
MRI-ESM2-0	Japan	160 × 320
NESM3	China	96 × 192

2.3. Definition of Gale Event in Observation and Model Simulation

In this study, the variable of instantaneous 10 m wind gust from ERA5 is used to define a gale day with at least one gale event (instantaneous wind speeds reach or exceed 17.0 m/s) in the 24 h grid. In order to investigate the daily and seasonal variations of gale events, we first sum gale events for all grids in North China and then count the proportions of hourly gale events in each day or monthly gale events in each year between 1980 and 2021. Due to the lack of hourly outputs from ESMs, we define a gale day with a daily maximum near-surface wind speed reaching or exceeding 17.0 m/s for future projections of gale weather events in North China.

2.4. Bias Correction of Model Simulations

ESM is an essential tool to project future climate change, but large uncertainties and biases were revealed by many previous climate change studies [33,38]. Therefore, before projecting the temporal and spatial changes of gale events in North China, we apply the quantile delta mapping (QDM) technique to correct daily maximum near-surface wind speed from model simulation in historical and future periods using the ERA5 reanalysis [39]. The QDM technique is developed to apply the same empirical cumulative distribution function (CDF) for model simulations and observations and to maintain the future change signal in climate change projections. For a given meteorological variable, the QDM method can be described as follows:

(1) We obtain the non-exceedance probability of x:

$$\varepsilon(t) = F_{s,p}^{(t)}\left[x_{m,f}(t)\right], \varepsilon(t) \in \{0,1\} \quad (1)$$

where $x_{m,p}(t)$ is the simulated (denoted by the subscript s) value at time t in the future period (denoted by the subscript f); $F_{s,f}^{(t)}$ is the time-dependent CDF of $x_{s,f}$.

(2) We calculate the absolute changes in quantiles between the future and calibration periods using the inverse CDFs in the future and calibration periods, $F_{s,f}^{(t)-1}$ and $F_{s,c}^{(t)-1}$:

$$\Delta_m(t) = F_{m,p}^{(t)-1}[\varepsilon(t)] - F_{m,c}^{(t)-1}[\varepsilon(t)] \quad (2)$$

(3) We correct the simulated ε quantile values at time t in future periods using the inverse CDF calculated from observations in the calibration period, $F_{o,c}^{(t)-1}$:

$$\hat{x}(t) = F_{o,c}^{(t)-1}[\varepsilon(t)] \quad (3)$$

(4) We obtain the bias-corrected simulations of $x_{m,p}$ at time t by adding the change signal in quantiles $\Delta_m(t)$ to the corrected quantile value $\hat{x}(t)$:

$$x_{corrected,s,f} = \hat{x}(t) + \Delta_m(t) \quad (4)$$

To validate the skill of the QDM technique independently, we divide historical observations into two segments. The 1980–2004 segment is defined as the calibration period, and the 2005–2014 segment is applied to validate the skill of the QDM technique in correcting the simulated daily maximum near-surface wind speed in North China. For future simulations under the SSP1-2.6 and SSP2-4.5 scenarios, 35-year (1980–2014) observations are defined as the calibration period to correct the projected daily maximum near-surface wind speed. In this study, the QDM technique is used for each model simulation separately, and an ensemble mean of eight ESMs is used to investigate the changes of gale events in North China by the mid-to-late 21st century under two SSPs scenarios.

3. Results

3.1. Daily and Seasonal Variations of Gale Events

Figure 1 shows the seasonal and daily variations of gale events between 1980 and 2021 in North China. It is seen that the gale events exhibit strong temporal variations in North China. For seasonal variation (Figure 2a), the gale events exhibit double peaks, with the largest peak (~20%) in April and the second peak (8%) in October. Such double peaks of gale events are mainly attributed to frequent Mongolian cyclones in spring and autumn [21,40,41]. Between June and July, the frequency of gale events reaches its minimum, accounting for only 3% of the annual total. For daily variation (Figure 2b), the gale events show a single peak with a maximum from 10:00 to 16:00 local time in North China. The largest frequency of gale events reaches > 12% in 13:00–14:00 local time in North China, which is related to the down sent momentum [42,43]. Generally, after the ground is heated in the afternoon, the enhanced vertical exchange of air results in gales being transmitted from high levels to the ground.

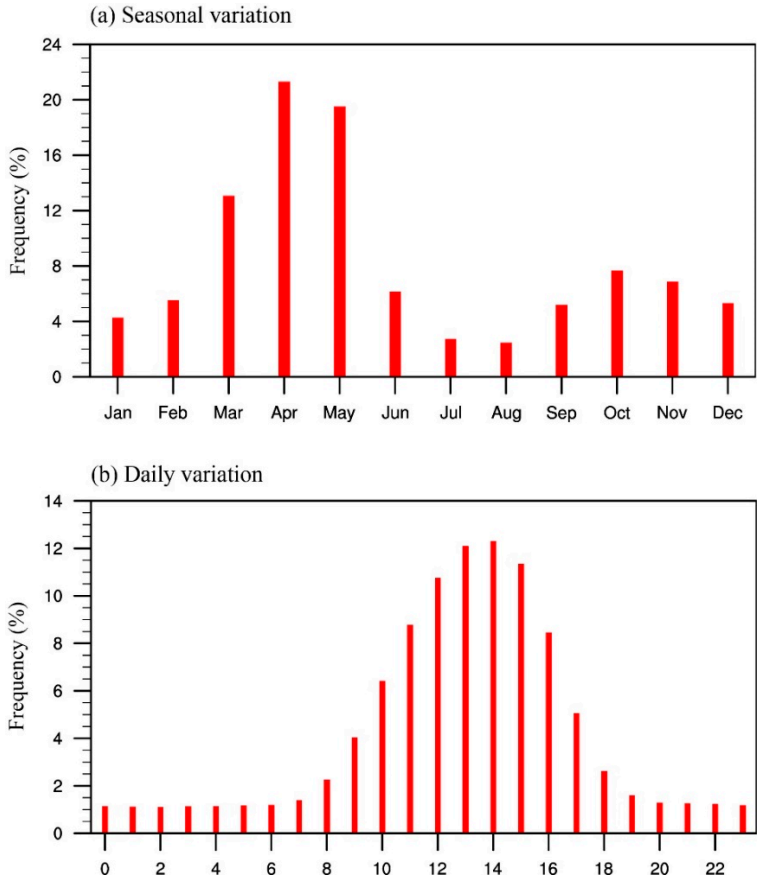

Figure 2. Seasonal (**a**) and daily (**b**) variations of gale events between 1980 and2021 in North China.

Observations revealed that the wind speed in North China suffered a decadal change in the past three decades, with a decline from 1990 and a recovery from 2008 [44]. Here, we further investigate the decadal change in temporal variation of gale events between 1980 and 2021 (Figure 3). From the 1980s to the 2010s, the gale events show a significant decreasing trend in April and June in North China (Figure 3a). On the contrary, an increasing trend of gale events in North China occurred in December from the 1980s to the 2010s. The largest frequency of gale events in March was found in the 2000s, but the largest frequency in September and October was found in the 1990s. In addition, the frequencies of gale events in May and November in North China decreased in the 1990s but reversed in the 2010s. For daily variation, the maximum gale events in North China occurred between 9:00

and 16:00 local time from the 1980s to the 2010s (Figure 3b). However, we find that gale events in North China decrease during the night and increase in the day, suggesting a shift from nighttime to daytime between the 1980s and 2010s.

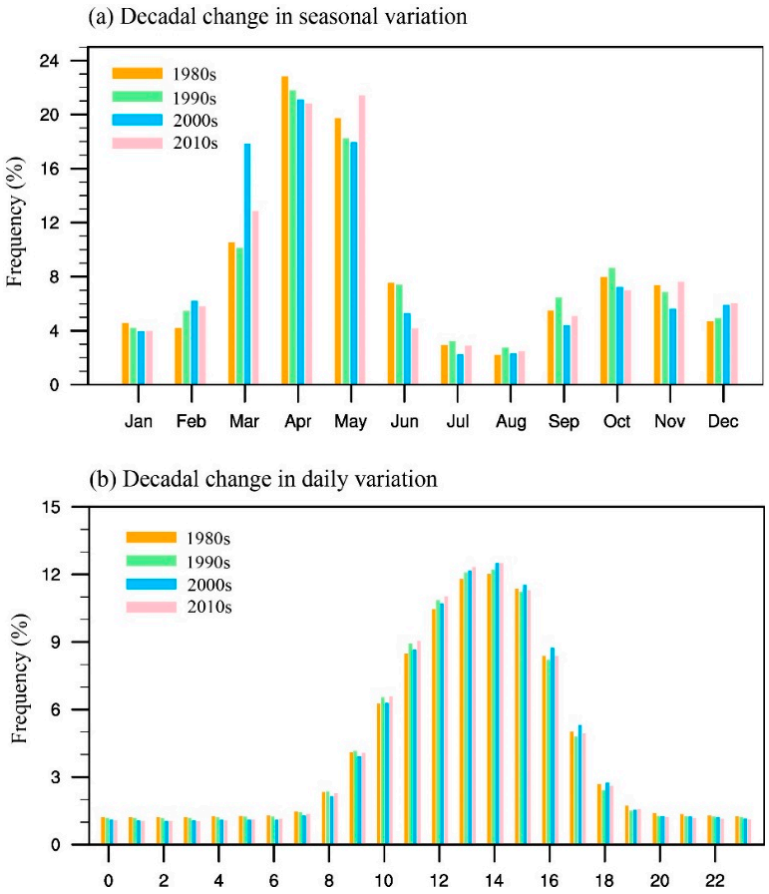

Figure 3. Decadal changes in seasonal (**a**) and daily (**b**) variations of gale events between 1980 and 2021 in North China. The orange, green, blue, and red bars represent the 1980s, 1990s, 2000s, and 2010s, respectively.

3.2. Model Evaluation of Gale Events in North China

In this study, we use eight ESMs from the CMIP6 to project the changes in gale events in North China by the end of the 21st century. We first evaluate the performance of ESMs in simulating observed gale events in North China in the historical period (2005–2014) (Figure 4). The results revealed North China's large spatial heterogeneity of gale events (Figure 4a). The large annual gale days of >25 are found in central Inner Mongolia, northern Hebei, and northwestern Beijing, where frequent weather systems occur. However, the annual gale days are smaller than 10 days in southern Shanxi province, Tianjin, and southeastern Beijing. Additionally, there is a narrow gale belt in the greater Khingan mountains, where the annual gale days are larger than 40 days. Compared to observations, the model simulations significantly underestimate the gale events in North China (Figure 4b). Especially in the central Inner Mongolia province, the underestimation reaches 20 days/year, suggesting that there are large uncertainties in simulated gale events using ESMs in North China. Therefore, we apply the QDM method to correct model simulations before projecting future changes in gale events in North China. It is seen that the bias-corrected model simulations reproduce the spatial pattern of gale events in North China with a high correlation coefficient of 0.98 and a low absolute bias of 0.6 days/year (Figure 4c). The above evaluation results demonstrate that the QDM method significantly improves the confidence level of model simulations from ESMs in simulating gale events in North

China. Therefore, we apply the QDM method to correct future projections under three SSP scenarios and project the changes in gale events in North China by the end of the 21st century in the following sections.

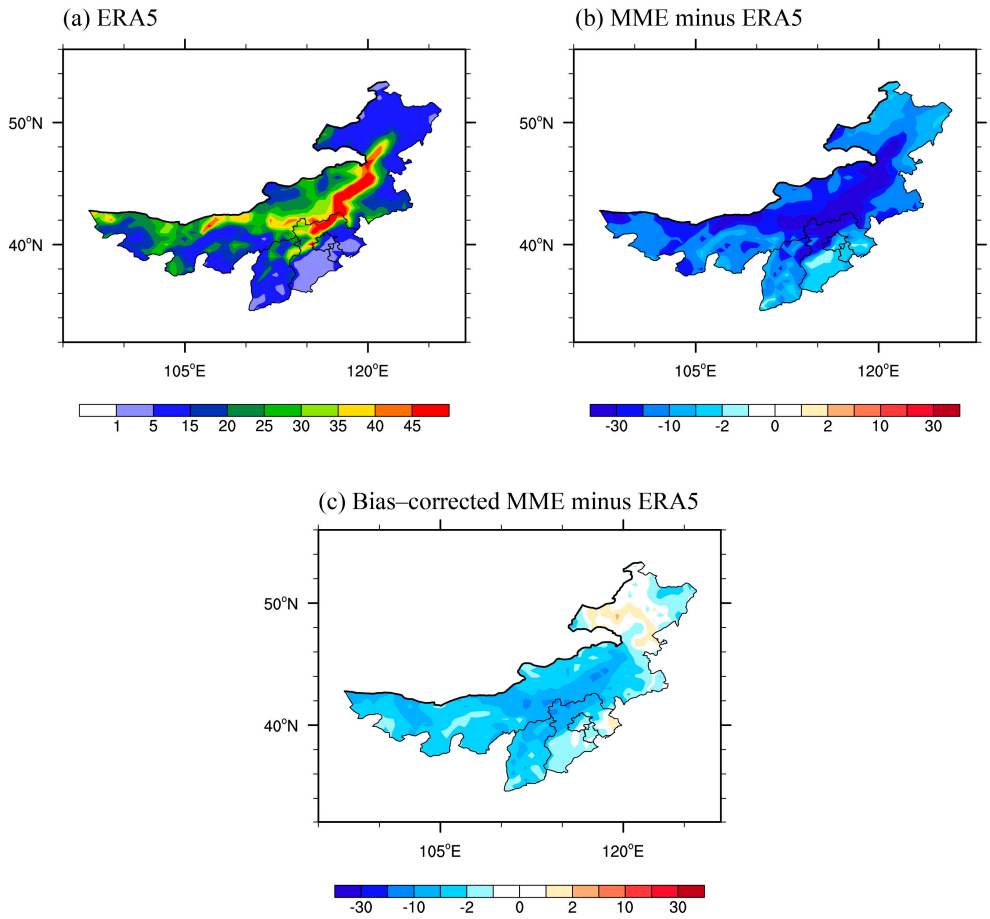

Figure 4. Evaluation of ESMs performance simulating gale events in North China between 2005 and 2014. (**a**) Observed annual days of gale; (**b**) the difference of annual days of gale between ensemble mean (MME) of eight ESMs and observation; and (**c**) the difference of annual days of gale between bias-corrected ensemble mean (MME) of eight ESMs and observation.

3.3. Projection of Gale Events in North China

Projection of gale events can provide essential information for planning aviation, renewable, and agriculture in the future. Figure 5 shows the temporal variation of gale events in North China in the historical period (1980–2014) and future period (2015–2100) under two SSP scenarios. Overall, regional mean gale events exhibit a decreasing trend in North China in the historical period. On an interdecadal scale, gale events in North China show a decadal reversal in about 2006, decreasing between 1980 and 2006 but increasing between 2007 and 2014. Such decadal reversal was also revealed in wind speed in North China [44,45]. In future periods, the projected gale events in North China will continue to decrease under the SSP1-2.6 and SSP2-4.5 scenarios. In the mid-21st century, there are limited differences in gale events in North China between the SSP1-2.6 and SSP2-4.5 scenarios. However, the decreasing gale events in the SSP2-4.5 scenario are significantly larger than that in the SSP1-2.6 scenario by the end of the 21st century relative to the historical period, suggesting fewer gale events in North China in a warmer climate.

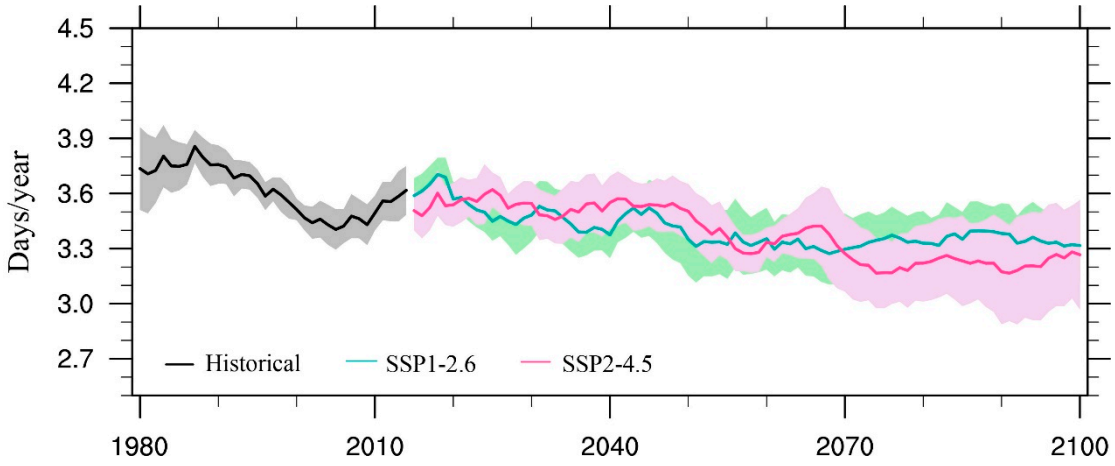

Figure 5. Time series of gale events in North China in historical (black line) and future periods. The green and red lines represent projected gale events in North China under SSP1-2.6 and SSP2-4.5 scenarios, respectively. The shadings represent one standard deviation of eight ESMs.

Although regional mean gale events in North China will decrease substantially in the future, there are obvious differences in magnitude on a regional scale (Figure 6). In the mid-21st century, the changes in annual gale events in North China under the SSP1-2.6 scenario relative to the historical period show large spatial heterogeneity. The largest decrease of >3 days/year is found in northern Hebei province, followed by 1–2 days/year in central Inner Mongolia and Shanxi province. In southwestern and northeastern Inner Mongolia, the changes are very small and lower than the significant level (Figure 6a). In the SSP2-4.5 scenario, the decreased gale events in the mid-21st century relative to the historical period are slightly smaller than that in SSP1-2.6 (Figure 6b). On a regional scale, the gale events increased slightly in Hebei province in the mid-21st century under the SSP2-4.5 scenario relative to the historical period. Compared to limited changes in the SSP1-2.6 scenario, the gale events in northeastern Inner Mongolia show a large decrease in the mid-21st century under the SPP2-4.5 scenario. Compared to the mid-21st century, the gale events are further decreased by the end of the 21st century under the SSP1-2.6 and SSP2-4.5 scenarios. Furthermore, there are large differences between the SSP1-2.6 and SSP2-4.5 scenarios by the end of the 21st century (Figure 6c vs. 6d). A large decline of gale events in North China is found in the SSP2-4.5 scenario rather than the SSP1-2.6 scenario by the end of 21st century. Especially in the greater Khingan mountains, the gale events are projected to decrease by >5 days/year by the end of the 21st century under the SSP2-4.5 scenario relative to the historical period. On the contrary, there are limited changes in gale events in southern Shanxi and Hebei provinces by the end of the 21st century under the SSP2-4.5 scenario relative to the historical period. The above analysis shows large scenario dependence and spatial heterogeneity of future gale events in North China relative to the historical period.

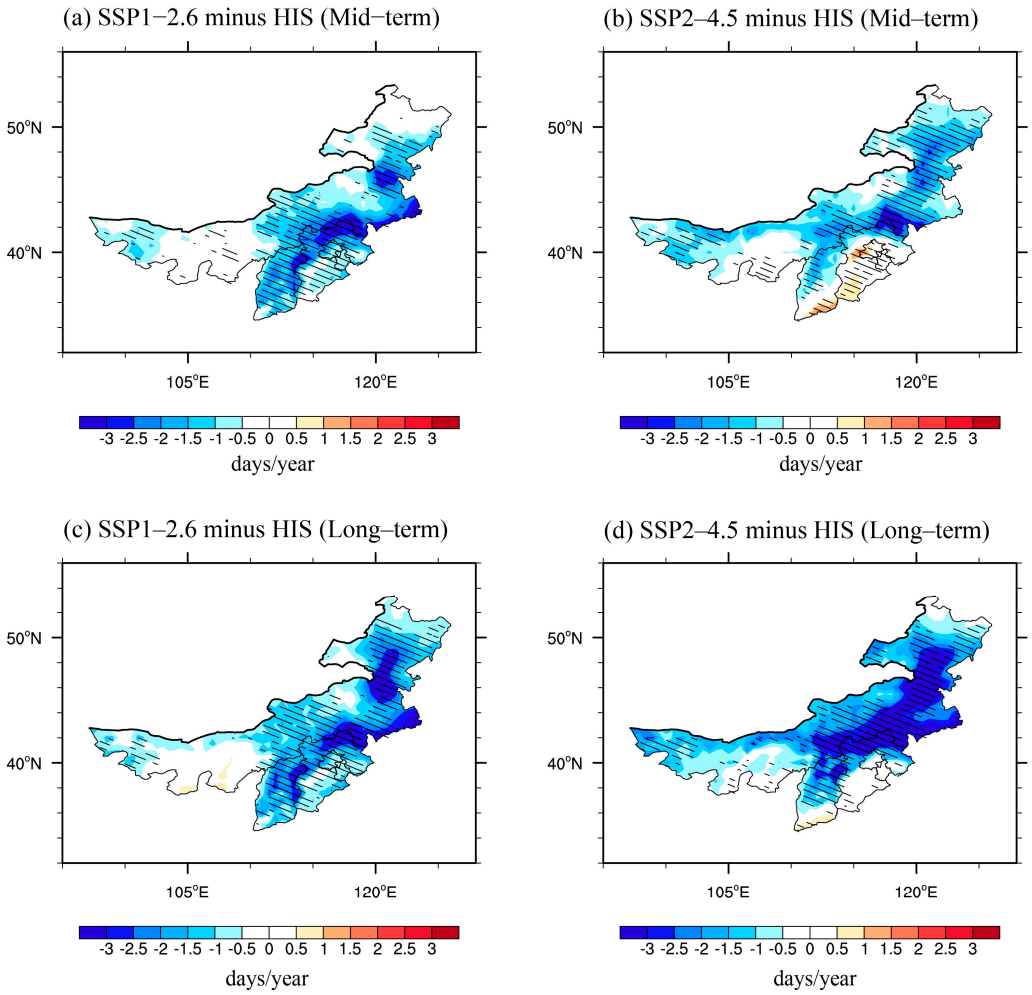

Figure 6. Spatial changes of gale events in North China in the short-term (2041–2060, (**a**,**b**)) and long-term (2081–2100, (**c**,**d**)) under the SSP1-2.6 (**a**,**c**) and the SSP2-4.5 (**b**,**d**) scenarios relative to the historical period (HIS, 1980–2014). Hatched regions represent a statistically robust change, defined here as at least six of the eight ESMs agreeing on the change direction.

4. Summary and Discussion

Gale is an important weather extreme that seriously threatens the ecosystem and economy [46,47]. In this study, we apply the ERA5 reanalysis with a high spatiotemporal resolution to investigate the spatial–temporal changes of gale events from 1980 to 2021 in North China. The gale events mainly occurred in central Inner Mongolia province, northern Hebei province, and northwestern Beijing, with >25 days per year. In the last four decades, gale events in North China exhibit an obvious decadal reversal, decreasing between 1980 and 2006 but increasing between 2007 and 2014. Furthermore, gale frequency in North China shows strong temporal variations, with a maximum in spring (March–May) and daytime (9:00–16:00 local time). Model simulations reveal that the gale events continuously decreased in the mid and late 21st century under the SSP1-2.6 and SSP2-4.5 scenarios relative to the historical period.

Compared to Shi et al. [28], which reported a similar decreasing trend of gale weather events in China from 1959 to 2014, our study provides some new insights, including the daily and seasonal variations and future projection of gale events based on the ERA5 analysis and multi-model simulations from CMIP6. Meanwhile, in contrast to most climate extremes becoming more frequent, gale events show a significant decreasing trend in a warmer climate, which is possibly related to decreasing wind speed in North China [44,45]. These findings are valuable for planning aviation, renewables, and agriculture in the future.

Our results have potential applications for flights, energy, and air quality. Firstly, gale weather can affect the takeoff and landing process of flights [48]. Strong crosswinds or gusts may cause difficulties in flight control and increase the risk of takeoff and landing accidents. Therefore, when the wind speed exceeds the maximum allowable value, the airline may cancel, delay, or change the route of the flight [49]. The temporal variations from this study can guide airlines in arranging flights in order to reduce economic losses. Secondly, strong winds may pose challenges to the structure of the wind turbine [50,51]. If the wind speed exceeds the limit range that the wind turbine can withstand, it may lead to serious consequences, such as blade breakage and tower overturning. Therefore, it is necessary to increase the dependence on photovoltaics in gale seasons such as April and October to ensure energy security. Finally, strong winds can bring large amounts of mineral dust aerosols from the Gobi Desert across southern Mongolia, causing serious environmental problems in North China [20,52]. In the last four decades, the decadal reversal of gale events in North China can account for part of the decadal changes in sand and dust storms.

Our study is subject to some limitations. First, we only project gale days in North China, not daily and seasonal variations, mainly because of the lack of high temporal and spatial outputs from CMIP6. In the future, the hourly outputs of ESMs from CMIP6 are required to project the daily and seasonal variations of gale events further by the mid-to-late 21st century. Second, we use a horizontal resolution of $0.5^\circ \times 0.5^\circ$ to investigate the changes in gale days in North China in historical and future periods. We chose this resolution because the resolutions of ESMs are relatively lower (Table 1). At present, the resolution of 0.5–1.0° is widely used in regional climate change projection [36,53]. We acknowledge that this resolution can induce biases for climate change projection. Therefore, we can downscale the model results using statical and dynamic methods to reduce the uncertainty of projection in future gale days in North China. Finally, our study provides a climatological analysis of gale weather events in North China in historical and future periods. Similar to other climate extreme studies [2,54–57], this study demonstrates a decreasing trend of gale events in a warmer climate, but the physical mechanisms are lacking. The formation of gale weather events is complicated and related to many weather and climate systems; therefore, we can cluster different types of gale events related to a specific weather system and investigate the possible reason behind decreasing gale events in North China in future studies.

Author Contributions: R.Y. and Q.L. contributed to the design and data analysis. R.Y. wrote the draft of the manuscript and received valuable comments from Q.L., L.W., M.H. and Y.H. All authors have read and agreed to the published version of the manuscript.

Funding: This study was supported by the Beijing Natural Science Foundation (No. 8232034).

Institutional Review Board Statement: Not applicable.

Informed Consent Statement: Not applicable.

Data Availability Statement: The ERA5 analysis supporting the conclusions in this study was obtained from the fifth-generation reanalysis from the European Centre for Medium-Range Weather Forecasts (https://www.ecmwf.int/en/forecasts/dataset/ecmwf-reanalysis-v5) (accessed on 1 January 2023). The simulations from eight CMIP6 ESMs can be downloaded at https://esgf-node.llnl.gov/projects/cmip6/ (accessed on 1 January 2023).

Conflicts of Interest: The authors declare no conflict of interest.

References

1. IPCC: Climate Change 2021: The Physical Science Basis. *Contribution of Working Group I to the Sixth Assessment Report of the Intergovernmental Panel on Climate Change, 2021*; IPCC: Geneva, Switzerland, 2021.
2. Wang, Z.; Lin, L.; Yang, M.; Xu, Y. The effect of future reduction in aerosol emissions on climate extremes in China. *Clim. Dyn.* **2016**, *47*, 2885–2899. [CrossRef]
3. Chen, R.; Wen, Z.; Lu, R.; Wang, C. Causes of the Extreme Hot Midsummer in Central and South China during 2017: Role of the Western Tropical Pacific Warming. *Adv. Atmos. Sci.* **2019**, *36*, 465–478. [CrossRef]

4. Wei, L.; Xin, X.; Li, Q.; Wu, Y.; Tang, H.; Li, Y.; Yang, B. Simulation and projection of climate extremes in China by multiple Coupled Model Intercomparison Project Phase 6 models. *Int. J. Clim.* **2023**, *43*, 219–239. [CrossRef]
5. Zhang, Y.; You, Q.; Ullah, S.; Chen, C.; Shen, L.; Liu, Z. Substantial increase in abrupt shifts between drought and flood events in China based on observations and model simulations. *Sci. Total. Environ.* **2023**, *876*, 162822. [CrossRef] [PubMed]
6. Mukherjee, S.; Mishra, A.K. Increase in Compound Drought and Heatwaves in a Warming World. *Geophys. Res. Lett.* **2021**, *48*, e2020GL090617. [CrossRef]
7. Almazroui, M.; Saeed, F.; Saeed, S.; Ismail, M.; Ehsan, M.A.; Islam, M.N.; Abid, M.A.; O'brien, E.; Kamil, S.; Rashid, I.U.; et al. Projected Changes in Climate Extremes Using CMIP6 Simulations Over SREX Regions. *Earth Syst. Environ.* **2021**, *5*, 481–497. [CrossRef]
8. Chen, H.; Sun, J. Significant Increase of the Global Population Exposure to Increased Precipitation Extremes in the Future. *Earth's Futur.* **2021**, *9*, e2020EF001941. [CrossRef]
9. Dahl, K.; Licker, R.; Abatzoglou, J.T.; Declet-Barreto, J. Increased frequency of and population exposure to extreme heat index days in the United States during the 21st century. *Environ. Res. Commun.* **2019**, *1*, 075002. [CrossRef]
10. Zhang, W.; Zhou, T. Significant Increases in Extreme Precipitation and the Associations with Global Warming over the Global Land Monsoon Regions. *J. Clim.* **2019**, *32*, 8465–8488. [CrossRef]
11. Ridder, N.N.; Ukkola, A.M.; Pitman, A.J.; Perkins-Kirkpatrick, S.E. Increased occurrence of high impact compound events under climate change. *Npj Clim. Atmos. Sci.* **2022**, *5*, 3. [CrossRef]
12. Heinonen, T.; Pukkala, T.; Ikonen, V.-P.; Peltola, H.; Gregow, H.; Venäläinen, A. Consideration of strong winds, their directional distribution and snow loading in wind risk assessment related to landscape level forest planning. *For. Ecol. Manag.* **2011**, *261*, 710–719. [CrossRef]
13. Li, S.; Tse, K.; Weerasuriya, A.; Chan, P. Estimation of turbulence intensities under strong wind conditions via turbulent kinetic energy dissipation rates. *J. Wind. Eng. Ind. Aerodyn.* **2014**, *131*, 1–11. [CrossRef]
14. Storer, L.N.; Williams, P.D.; Gill, P.G. Aviation Turbulence: Dynamics, Forecasting, and Response to Climate Change. *Pure Appl. Geophys.* **2019**, *176*, 2081–2095. [CrossRef]
15. Li, D.; Feng, J.; Dosio, A.; Qi, J.; Xu, Z.; Yin, B. Historical Evaluation and Future Projections of 100-m Wind Energy Potentials Over CORDEX-East Asia. *J. Geophys. Res. Atmos.* **2020**, *125*, e2020JD032874. [CrossRef]
16. Lai, L.-W. The relationship between extreme weather events and crop losses in central Taiwan. *Theor. Appl. Clim.* **2018**, *134*, 107–119. [CrossRef]
17. Leung, A.C.W.; Gough, W.A.; Butler, K.A.; Mohsin, T.; Hewer, M.J. Characterizing observed surface wind speed in the Hudson Bay and Labrador regions of Canada from an aviation perspective. *Int. J. Biometeorol.* **2022**, *66*, 411–425. [CrossRef] [PubMed]
18. Niacsu, L.; Sfica, L.; Ursu, A.; Ichim, P.; Bobric, D.E.; Breaban, I.G. Wind erosion on arable lands, associated with extreme blizzard conditions within the hilly area of Eastern Romania. *Environ. Res.* **2019**, *169*, 86–101. [CrossRef] [PubMed]
19. Wei, X.; Wu, X.; Wang, D.; Wu, T.; Li, R.; Hu, G.; Zou, D.; Bai, K.; Ma, X.; Liu, Y.; et al. Spatiotemporal variations and driving factors for potential wind erosion on the Mongolian Plateau. *Sci. Total Environ.* **2023**, *862*, 160829. [CrossRef]
20. Gui, K.; Yao, W.; Che, H.; An, L.; Zheng, Y.; Li, L.; Zhao, H.; Zhang, L.; Zhong, J.; Wang, Y.; et al. Record-breaking dust loading during two mega dust storm events over northern China in March 2021: Aerosol optical and radiative properties and meteorological drivers. *Atmos. Meas. Tech.* **2022**, *22*, 7905–7932. [CrossRef]
21. Yin, Z.; Wan, Y.; Zhang, Y.; Wang, H. Why super sandstorm 2021 in North China? *Natl. Sci. Rev.* **2022**, *9*, nwab165. [CrossRef]
22. Wang, E.; Yu, Q.; Wu, D.; Xia, J. Climate, agricultural production and hydrological balance in the North China Plain. *Int. J. Clim.* **2008**, *28*, 1959–1970. [CrossRef]
23. Xin, Y.; Tao, F. Developing climate-smart agricultural systems in the North China Plain. *Agric. Ecosyst. Environ.* **2020**, *291*, 106791. [CrossRef]
24. Sun, H.; Luo, Y.; Zhao, Z.; Chang, R. The Impacts of Chinese Wind Farms on Climate. *J. Geophys. Res. Atmos.* **2018**, *123*, 5177–5187. [CrossRef]
25. Xu, Z.; Chen, S.X.; Wu, X. Meteorological Change and Impacts on Air Pollution: Results from North China. *J. Geophys. Res. Atmos.* **2020**, 125. [CrossRef]
26. Li, J.; Hao, X.; Liao, H.; Wang, Y.; Cai, W.; Li, K.; Yue, X.; Yang, Y.; Chen, H.; Mao, Y.; et al. Winter particulate pollution severity in North China driven by atmospheric teleconnections. *Nat. Geosci.* **2022**, *15*, 349–355. [CrossRef]
27. Tong, P.F.; Chen, S.X.; Tang, C.Y. Detecting and Evaluating Dust-Events in North China with Ground Air Quality Data. *Earth Space Sci.* **2022**, *9*, e2021EA001849. [CrossRef]
28. Shi, J.; Wen, K.; Cui, L. Temporal and spatial variations of high-impact weather events in China during 1959–2014. *Theor. Appl. Clim.* **2017**, *129*, 385–396. [CrossRef]
29. Fan, W.; Liu, Y.; Chappell, A.; Dong, L.; Xu, R.; Ekström, M.; Fu, T.-M.; Zeng, Z. Evaluation of Global Reanalysis Land Surface Wind Speed Trends to Support Wind Energy Development Using In Situ Observations. *J. Appl. Meteorol. Clim.* **2021**, *60*, 33–50. [CrossRef]
30. Huang, J.; Yin, J.; Wang, M.; He, Q.; Guo, J.; Zhang, J.; Liang, X.; Xie, Y. Evaluation of Five Reanalysis Products with Radiosonde Observations Over the Central Taklimakan Desert During Summer. *Earth Space Sci.* **2021**, *8*, e2021EA001707. [CrossRef]
31. Taszarek, M.; Allen, J.T.; Marchio, M.; Brooks, H.E. Global climatology and trends in convective environments from ERA5 and rawinsonde data. *Npj Clim. Atmos. Sci.* **2021**, *4*, 35. [CrossRef]

32. Yan, Y.; Xu, Y.; Yue, S. A high-spatial-resolution dataset of human thermal stress indices over South and East Asia. *Sci. Data* **2021**, *8*, 229. [CrossRef] [PubMed]
33. Lei, Y.; Wang, Z.; Wang, D.; Zhang, X.; Che, H.; Yue, X.; Tian, C.; Zhong, J.; Guo, L.; Li, L.; et al. Co-benefits of carbon neutrality in enhancing and stabilizing solar and wind energy. *Nat. Clim. Change* **2023**, *13*, 693–700. [CrossRef]
34. Wang, Z.L.; Lin, L.; Zhang, X.Y.; Zhang, H.; Liu, L.K.; Xu, Y.Y. Scenario dependence of future changes in climate extremes under 1.5 degrees C and 2 degrees C global warming. *Sci. Rep.* **2017**, *7*, 46432.
35. Lei, Y.D.; Yue, X.; Liu, Z.Y. Dipole response of early-summer rainfall in eastern China to 1.5 and 2.0 degrees C global warming. *Int. J. Climatol.* **2022**, *42*, 10009–10020.
36. Tian, C.; Yue, X.; Zhou, X.; Lei, Y.; Zhou, H.; Cao, Y. Projection of Long-Term Climate Change in China Under COVID-19 Recovery Emission Scenarios. *J. Geophys. Res. Atmos.* **2023**, *128*, e2023JD039197. [CrossRef]
37. O'Neill, B.C.; Tebaldi, C.; van Vuuren, D.P.; Eyring, V.; Friedlingstein, P.; Hurtt, G.; Knutti, R.; Kriegler, E.; Lamarque, J.-F.; Lowe, J.; et al. The Scenario Model Intercomparison Project (ScenarioMIP) for CMIP6. *Geosci. Model Dev.* **2016**, *9*, 3461–3482. [CrossRef]
38. Li, D.; Yuan, J.; Kopp, R.E. Escalating global exposure to compound heat-humidity extremes with warming. *Environ. Res. Lett.* **2020**, *15*, 064003. [CrossRef]
39. Cannon, A.J.; Sobie, S.R.; Murdock, T.Q. Bias Correction of GCM Precipitation by Quantile Mapping: How Well Do Methods Preserve Changes in Quantiles and Extremes? *J. Clim.* **2015**, *28*, 6938–6959. [CrossRef]
40. Li, J.; Hao, X.; Liao, H.; Yue, X.; Li, H.; Long, X.; Li, N. Predominant Type of Dust Storms That Influences Air Quality Over Northern China and Future Projections. *Earth's Futur* **2022**, *10*, e2022EF002649. [CrossRef]
41. Chen, S.; Zhao, D.; Huang, J.; He, J.; Chen, Y.; Chen, J.; Bi, H.; Lou, G.; Du, S.; Zhang, Y.; et al. Mongolia Contributed More than 42% of the Dust Concentrations in Northern China in March and April 2023. *Adv. Atmos. Sci.* **2023**, *40*, 1549–1557. [CrossRef]
42. Wu, Z.; Wang, S.; Shang, K.; Yang, Z.; Chen, F. The Characteristics of Momentum Transfer during a Cold Strong Wind Process. *J. Desert Res.* **2016**, *36*, 467–473.
43. Lan, C.; Xie, J.; Li, L.; Wang, B.; Yang, H.; Lu, J. Downward Momentum Flux: An Important Mechanism of Typhoon Maintaining Ground Destructive Force. *J. Geophys. Res. Atmos.* **2023**, *128*, e2022JD037470. [CrossRef]
44. Liu, Y.; Zeng, Z.; Xu, R.; Ziegler, A.D.; Jerez, S.; Chen, D.; Azorin-Molina, C.; Zhou, L.; Yang, X.; Xu, H.; et al. Increases in China's wind energy production from the recovery of wind speed since 2012. *Environ. Res. Lett.* **2022**, *17*, 114035. [CrossRef]
45. Zha, J.; Shen, C.; Zhao, D.; Wu, J.; Fan, W. Slowdown and reversal of terrestrial near-surface wind speed and its future changes over eastern China. *Environ. Res. Lett.* **2021**, *16*, 034028. [CrossRef]
46. Zhang, Y.; Lam, J.S.L. Estimating the economic losses of port disruption due to extreme wind events. *Ocean Coast. Manag.* **2015**, *116*, 300–310. [CrossRef]
47. Coccolo, S.; Mauree, D.; Naboni, E.; Kaempf, J.; Scartezzini, J.-L. On the impact of the wind speed on the outdoor human comfort: A sensitivity analysis. *Energy Procedia* **2017**, *122*, 481–486. [CrossRef]
48. Shamoun-Baranes, J.; van Loon, E.; Liechti, F.; Bouten, W. Analyzing the effect of wind on flight: Pitfalls and solutions. *J. Exp. Biol.* **2007**, *210*, 82–90. [CrossRef] [PubMed]
49. Burnett, N.P.; Badger, M.A.; Combes, S.A. Wind and route choice affect performance of bees flying above versus within a cluttered obstacle field. *PLoS ONE* **2022**, *17*, e0265911. [CrossRef]
50. Chen, X.; Liu, L.; Huang, W. The detection and prediction for oil spill on the sea based on the infrared images. *Infrared Phys. Technol.* **2016**, *77*, 391–404. [CrossRef]
51. Chou, J.-S.; Ou, Y.-C.; Lin, K.-Y.; Wang, Z.-J. Structural failure simulation of onshore wind turbines impacted by strong winds. *Eng. Struct.* **2018**, *162*, 257–269. [CrossRef]
52. Yang, L.; Zhang, S.; Huang, Z.; Yang, Y.; Wang, L.; Han, W.; Li, X. Characteristics of Dust Events in China from 2015 to 2020. *Atmosphere* **2021**, *12*, 952. [CrossRef]
53. Zhou, B.; Xu, Y.; Wu, J.; Dong, S.; Shi, Y. Changes in temperature and precipitation extreme indices over China: Analysis of a high-resolution grid dataset. *Int. J. Clim.* **2016**, *36*, 1051–1066. [CrossRef]
54. Wang, Y.; Zhou, B.; Qin, D.; Wu, J.; Gao, R.; Song, L. Changes in Mean and Extreme Temperature and Precipitation over the arid Region of Northwestern China: Observation and Projection. *Adv. Atmos. Sci.* **2017**, *34*, 289–305. [CrossRef]
55. Niu, X.; Wang, S.; Tang, J.; Lee, D.-K.; Gutowski, W.; Dairaku, K.; McGregor, J.; Katzfey, J.; Gao, X.; Wu, J.; et al. Ensemble evaluation and projection of climate extremes in China using RMIP models. *Int. J. Clim.* **2018**, *38*, 2039–2055. [CrossRef]
56. Avila-Diaz, A.; Benezoli, V.; Justino, F.; Torres, R.; Wilson, A. Assessing current and future trends of climate extremes across Brazil based on reanalyses and earth system model projections. *Clim. Dyn.* **2020**, *55*, 1403–1426. [CrossRef]
57. Lei, Y.; Wang, Z.; Zhang, X.; Che, H.; Yue, X.; Tian, C.; Zhong, J.; Guo, L.; Li, L.; Zhou, H. Avoided population exposure to extreme heat under two scenarios of global carbon neutrality by 2050 and 2060. *Environ. Res. Lett.* **2022**, *17*, 094041. [CrossRef]

Disclaimer/Publisher's Note: The statements, opinions and data contained in all publications are solely those of the individual author(s) and contributor(s) and not of MDPI and/or the editor(s). MDPI and/or the editor(s) disclaim responsibility for any injury to people or property resulting from any ideas, methods, instructions or products referred to in the content.